AIRESEARCH MANUFACTURING COMPANY
OF CALIFORNIA
A Division of The Garrett Corporation
2525 West 190th Street, Torrance, Calif. 90509

HYPERSONIC RESEARCH ENGINE PROJECT - PHASE II PRELIMINARY REPORT ON THE PERFORMANCE OF THE HRE/AIM AT MACH 6 (U)

DATA ITEM NO. 54.15
NASA CONTRACT NO. NAS1-6666

72-10251

ISSUED MAY 1975

(NASA-CR-122538) HYPERSONIC RESEARCH ENGINE PROJECT, PHASE 2. PRELIMINARY REPORT ON THE PERFORMANCE OF THE HRE/AIM AT MACH 6 (AiResearch Mfg. Co., Torrance, Calif.) 26 p HC $3.75 CSCL 21E G3/07

N75-24742

Unclas
25367

Number of pages 26

Original date November 6, 1974

Prepared by Y. H. Sun and W. C. Sabiro

Edited by N/A

Approved by E. G. Wolff
for Edward N. Barris
HRE Program Manager

Prepared for
National Aeronautics and Space Administration
Langley Research Center
Hampton, Virginia 23365

FOREWORD

This analytical report is submitted to the NASA Langley Research Center in compliance with Paragraph 5.7.3.2.1 of NASA Statement of Work I-4947-B (Revised).

The contents of this report were previously presented as a scientific paper before the JANNAF (Joint Army, Navy, NASA, and Air Force) Propulsion Conference held in San Diego, California, on October 22, 1974.

CONTENTS

	Page
ABSTRACT	1
INTRODUCTION	1
TEST FACILITY	2
DESCRIPTION OF AIM	4
SUBSONIC AND SUPERSONIC COMBUSTION	9
COMPONENT PERFORMANCE	9
OVERALL ENGINE INTERNAL PERFORMANCE	16
CONCLUSIONS	21
REFERENCES	21

ILLUSTRATIONS

Figure		Page
1	NASA Hypersonic Tunnel Facility	3
2	AIM Test Section Schematic	3
3	AIM Installed in Wind Tunnel	5
4	AIM Aerodynamic Contours	5
5	Copper Cowl Leading Edge After Completion of Tests	6
6	Heat Patterns Showing Injector Impingement	7
7	Altitude Mach Number Envelope	8
8	Subsonic and Supersonic Combustion	10
9	Inlet Pressure Distribution	10
10	AIM Combustor Efficiency Range	12
11	Combustor Total Pressure Recovery	12
12	Nozzle Performance	13
13	Unsymmetrical Shock Pattern at Combustor Exit	15
14	Temperature-Entropy Diagram for Supersonic Combustion	15
15	Comparison of Thrust Calculations	18
16	AIM Internal Performance	19
17	Thrust Distribution All Force Distribution	19
18	Hypersonic Ramjet Performance	20

PRELIMINARY REPORT ON THE PERFORMANCE OF NASA HYPERSONIC RESEARCH ENGINE (AIM/HRE) AT MACH 6 (U)

Yung H. Sun and Walter C. Sainio
AiResearch Manufacturing Company of California
Torrance, California

ABSTRACT

(U) This paper presents some test results of the Aerothermodynamic Integration Model (AIM) which was built under Hypersonic Research Engine Contract NAS1-6666, NASA Langley Research Center. A program was initiated in February 1967 to develop a hydrogen-fueled research-oriented scramjet for operation between Mach 3 and 8. The primary objectives were to investigate the internal aerothermodynamic characteristics of the engine to provide realistic design parameters for future hypersonic engine development as well as to evaluate the ground test facility and testing techniques. The engine was tested at the NASA Hypersonic Tunnel Facility (HTF) at the Plum Brook Station of the Lewis Research Center with synthetic air at Mach 5, 6, and 7. The hydrogen fuel was heated up to 1500°R prior to injection to simulate a regeneratively cooled system.

(C) Of the numerous investigations conducted, this paper presents only the engine and component performance at Mach 6. Inlet performance compared very well both with theory and with subscale model tests. Combustor efficiencies up to 95 percent were attained at an equivalence ratio of unity. Nozzle performance was lower than expected. The overall engine performance was computed using two different methods. The performance was also compared with test data from other sources.

INTRODUCTION

(U) This paper presents some test results at Mach 6 of the NASA Aerothermodynamic Integration Model (AIM). The AIM was designed, developed and built by AiResearch Manufacturing Company of California, under the Hypersonic Research Engine Contract with the NASA Langley Research Center. Work was initiated on the contract in February 1967. The basic objectives were to conduct ground-based and flight experiments which would provide realistic and useful information needed to advance the technology of hypersonic propulsion systems, and to evaluate requirements for future ground test facilities and experimental techniques. The AIM is a hydrogen-fueled research-oriented ramjet engine designed for operation at flight Mach numbers from 3 to 8. The engine size was selected primarily from the constraints imposed by the X-15 airplane which was originally scheduled as the flight test vehicle. The AIM was designed to operate with supersonic combustion at freestream Mach numbers from 6 to 8, and with subsonic combustion from Mach 3 to 6.

(U) A total of 6-1/2 months of engine testing has been completed with 110 minutes of running time accumulated. Among numerous investigations conducted, the following topics pertinent to a propulsion system at Mach 6 are reported herein.

1. Subsonic and supersonic combustion
2. Component performance
3. Engine cycle and efficiencies
4. Overall engine performance

TEST FACILITY

(U) The engine was tested at the NASA Hypersonic Tunnel Facility (HTF) at the Plum Brook Station of the Lewis Research Center. This facility was designed to be capable of true aerothermodynamic simulation of the flight environment at Mach 5, 6, and 7. The HTF incorporated a blowdown enclosed free-jet test section. The facility used an induction-heated, drilled-core graphite storage bed to raise the temperature of nitrogen to a nominal 4500°F at a maximum design pressure of 1200 psia. The nitrogen was mixed with ambient-temperature oxygen to produce synthetic air*. Ambient-temperature nitrogen was added along with the oxygen in the mixer at tunnel Mach numbers below 7 to control freestream total temperature and to supply the correct weight flow to the 42-inch exit-diameter free-jet nozzles. Altitude simulation was provided by a diffuser and a single-stage steam ejector as shown in Figure 1. The total length of this exhaust system was 183 ft.

(U) The test chamber was 25 ft in diameter. The facility nozzle and the diffuser duct penetrated the chamber wall through inflatable seals. A schematic of the engine and the test section is shown in Figure 2. The engine had a maximum cross-sectional area of approximately 50 percent of the facility nozzle. The shroud and the annular injector were installed to improve the tunnel starting and operational characteristics. The shroud channelled the tunnel flow around the model in order to lower the test chamber pressure. The annular ejector was used to inject cold nitrogen at the nozzle exit to increase the stream momentum in the tunnel nozzle boundary layer thereby preventing flow separation. The ring attached at the shroud entrance was used to restrict the reverse flow caused by the incident shock from the engine cowl lip. In the earlier runs the tunnel diffuser was choked. This situation was circumvented by reducing the diffuser cone angle. The back pressure in some test conditions was still high enough to form a shock between the engine and shroud, making the calculation of engine external drag extremely difficult. In severe cases, the shock would cause tunnel unstart.

*Small carbon particles were observed during tests. No attempt was made to assess the effect of the carbon particles on ignition or engine performance.

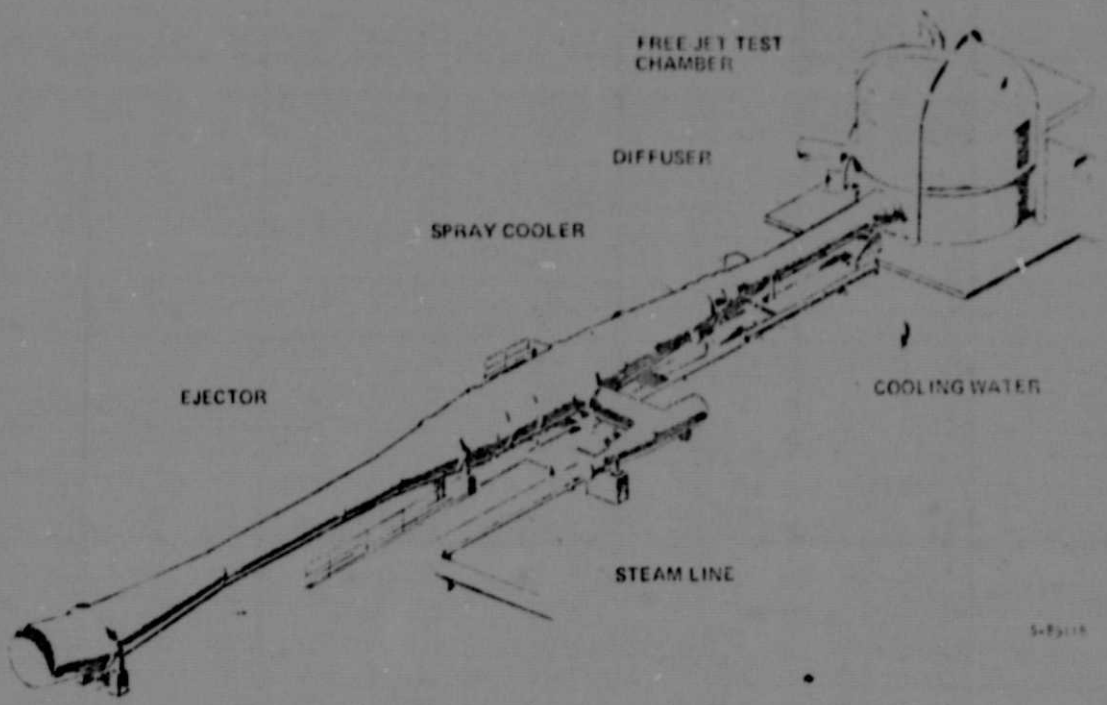

Figure 1. NASA Hypersonic Tunnel Facility
Title (U), figure (U)

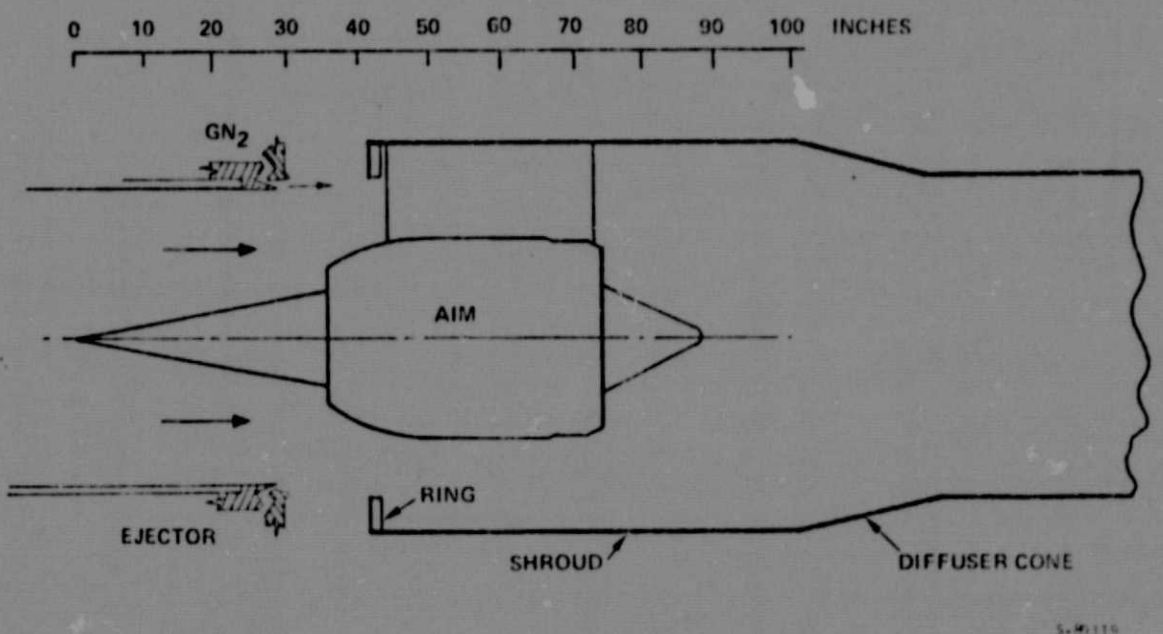

Figure 2. AIM Test Section Schematic
Title (U), figure (U)

(U) The data recording system consisted of an analog to digital converter capable of recording 400 channels of data on magnetic tape. The average sampling rate per channel was 5 times per second. Secondary data recording capability was provided by multi-channel oscillographs and strip-chart recorders. In addition, schlieren pictures between facility nozzle exit and shroud were displayed providing real time visual observation of tunnel operation. Motion pictures were also recorded during the run to assist in post-run analysis.

DESCRIPTION OF AIM

(U) The AIM is axisymmetric, water-cooled and uses hydrogen fuel. Figure 3 shows the engine when it was installed in the test cell. The engine consists basically of a two-shell welded structure. The shell adjacent to the hot gas was fabricated from nickel, and the cold side was fabricated from steel. The tips of the spike and the cowl leading edge were made from zirconium copper. The AIM weighs approximately 2200 pounds. Figure 4 shows the aerodynamic contours of the engine. The AIM has an inlet diameter of 18 inches, and the exit nozzle area is twice the inlet capture area. The overall length with the translating spike in the full-forward position is 91 inches. The engine contour was based on results from the subscale component tests (Ref. 1, 2, 3).

(U) In order to minimize the correction on the internal thrust measurement, the external cowl and leg fairings are supported separately from the thrust measuring system. Purge nitrogen was used in the cavity between the engine shroud and the outerbody. Because of unbalanced areas and flow restrictions inside the cavity, a large tare force was produced from the purge flow. This tare force was calibrated and correlated to determine the internal engine thrust.

(U) Inlet. The engine uses a mixed-compression inlet with a variable contraction ratio. Translation of the centerbody and a five-degree upsloping throat design were used to control the mass flow and to vary the contraction ratio.

(C) Most of the compression was accomplished by means of the spike which uses an initial 10-degree half-angle cone followed by an isentropic compression surface which turns the flow to a maximum angle of 20 deg. This design concept resulted in a low internal contraction ratio inlet which minimized the starting problem. The leading edge radii of the spike and cowl were 0.125 and 0.030 inches, respectively. The inlet design produced mass flow ratios of unity from Mach 6 to 8, and 0.86 and 0.70 for Mach 5 and 4, respectively. Figure 5 shows a portion of the copper cowl leading edge after the tests. The dented surface was caused by impingement of carbon particles from the induction heater.

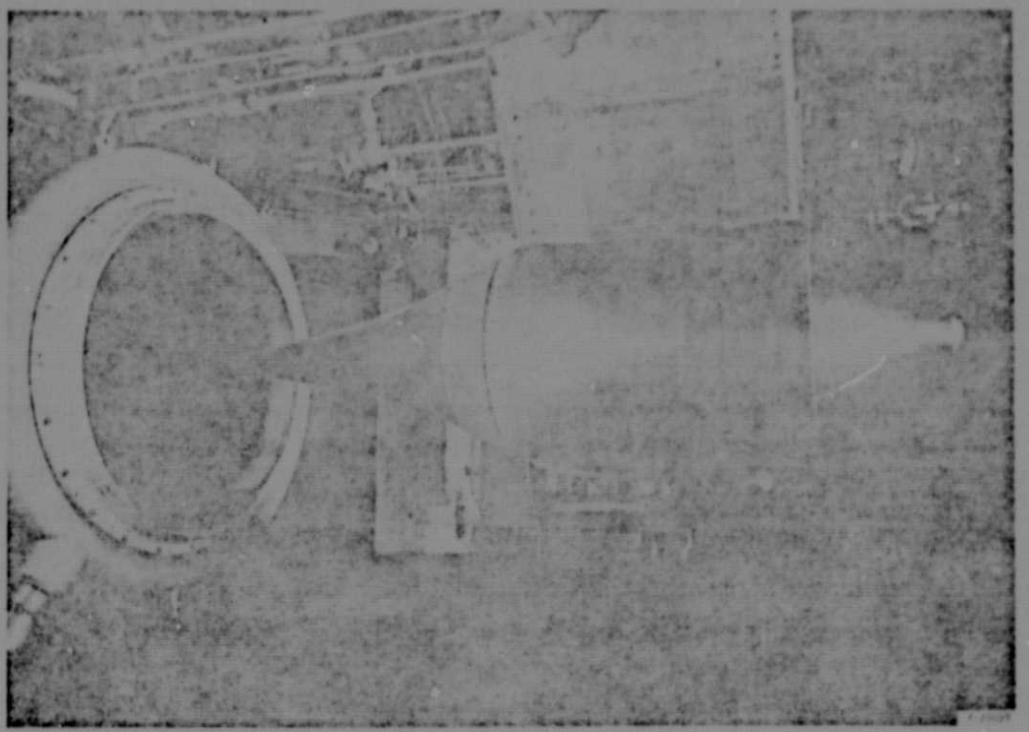

Figure 3. AIM Installed in Wind Tunnel
Title (U), figure (U)

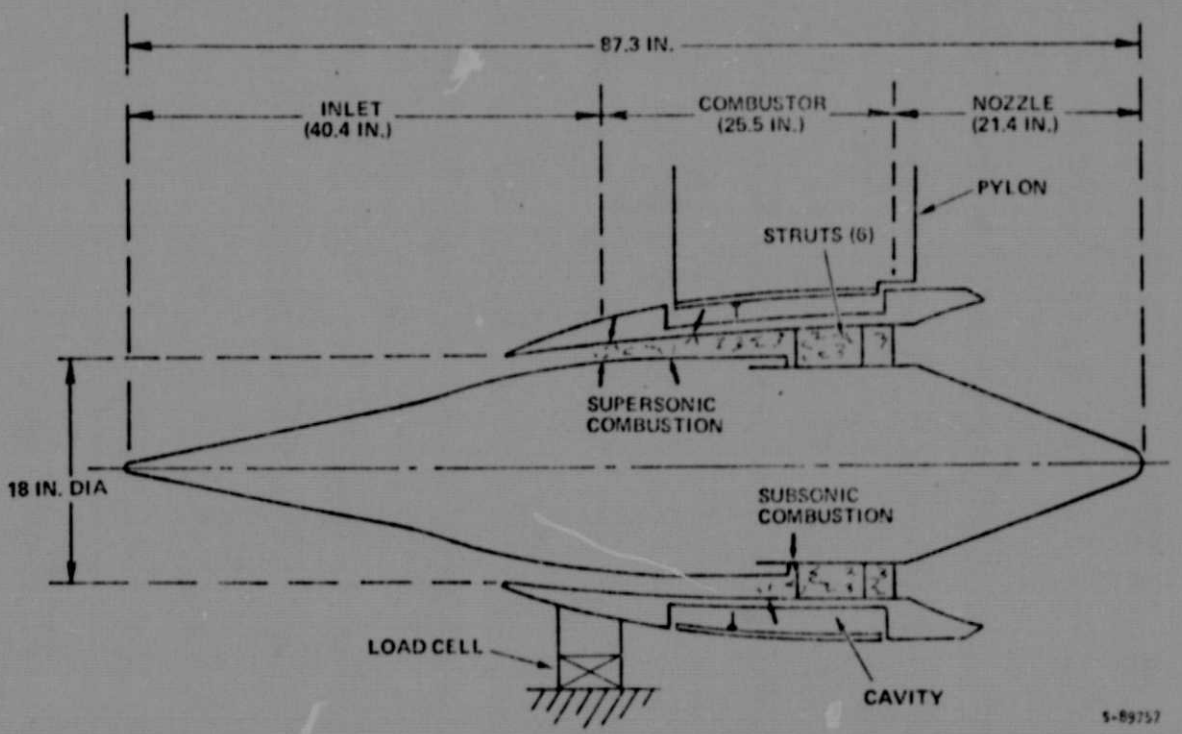

Figure 4. AIM Aerodynamic Contours
Title(U), figure (U)

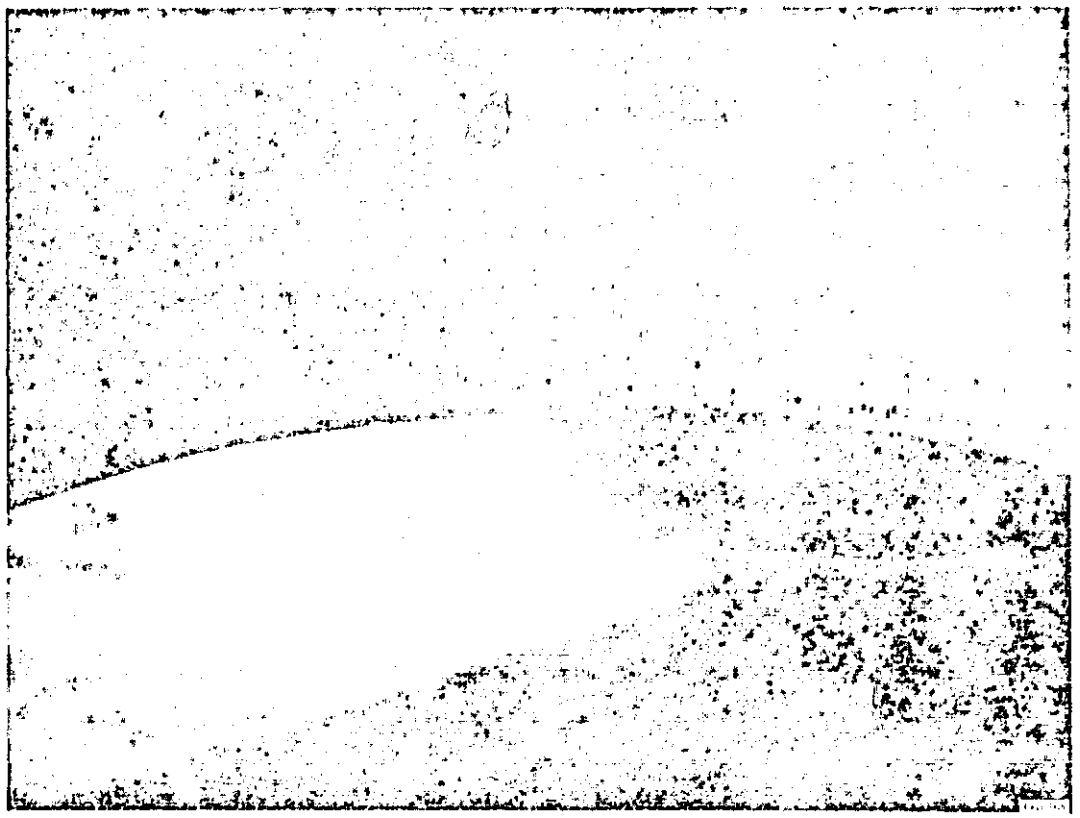

Fig. 5. Copper Cowl Leading Edge After Completion of Tests
Title (U), Figure (U)

(C) Combustor. The combustor has an overall useful length of 25.5 inches with an area ratio of 3.6. The combustor consists of three stages. The first two stages, a near constant area section followed by a diverging section, were used for supersonic combustion at higher flight Mach numbers and also for subsonic diffusion at lower Mach numbers. The third stage was used for subsonic combustion.

(U) At Mach 8, all fuel up to an equivalence ratio of one may be injected into the first stage. Because of spike translation, combustion occurs in a constant area section. For operation below Mach 8, fuel was to be injected into the first two stages in order to prevent thermal choking and inlet unstart.

(C) The step formed between the spike assembly and the inner shell is used as the flame stabilizer for subsonic combustion in the third stage. The maximum cross-section of the struts forms a geometric throat for subsonic combustion with an area reduction of five percent. The throat area was chosen to provide the best performance considering both subsonic and supersonic combustion. During subsonic combustion at Mach 4, the engine was designed so that the normal shock would stabilize near the inlet throat, while at Mach 6 the shock would move downstream near the step.

(U) The size and location of fuel injectors were selected to obtain optimum mixing through fuel penetration and jet spreading. The detailed injector design procedures were reported in Reference 2.

(U) In order to increase the mixing efficiency, the injectors in each stage were interdigitized in order to capture the maximum mixing area. In the final configuration, however, the injectors in the first stage were in line, i.e. opposed to each other. Consequently, mixing efficiency of the first stage was reduced. The consequence of this arrangement could not be assessed quantitatively. Figure 6 shows the injector impingement on the opposite walls.

(C) Nozzle. The AIM uses a fixed geometry annular nozzle which was selected as the configuration most compatible with the annular combustor design to provide best performance for flight Mach numbers from 3 to 8 (Ref. 4). It has an innerbody plug combined with an outerbody shroud to obtain the maximum permissible exit area. The shroud was an optimized contour with an exit angle of approximately 10 degrees. The plug was a 21.75 degree half-angle cone truncated at a radius of 2.5 inches. The nozzle area ratio was 5.5 with a pressure ratio of 110 at Mach 6. The constraint imposed on the exit area of the nozzle resulted in under-expanded operation above Mach 6.

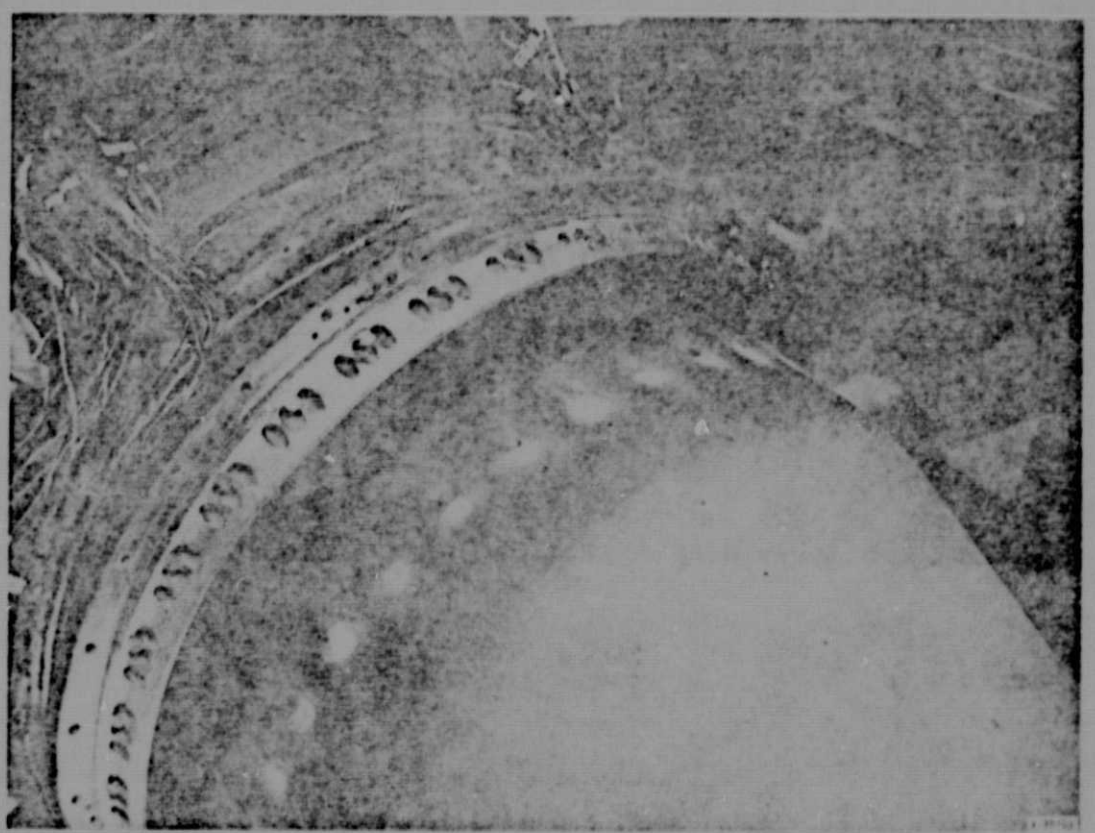

Fig. 6. Heat Patterns Showing Injector Impingement
Title (U), figure (U)

(U) Test Envelope. The engine was originally designed to operate within the altitude-Mach number envelope of the X-15-2 airplane. The constant dynamic pressure line of 1800 psf in Figure 7 represented the design altitudes at which the flight tests were planned. The line with a dynamic pressure of 900 psf represents the upper operating limits of this engine which is approximately 15,000 ft. above the design line. The points in Figure 7 were the flight conditions simulated in this program. Because of facility problems and time limitations, true temperature simulation of Mach 7 was not achieved.

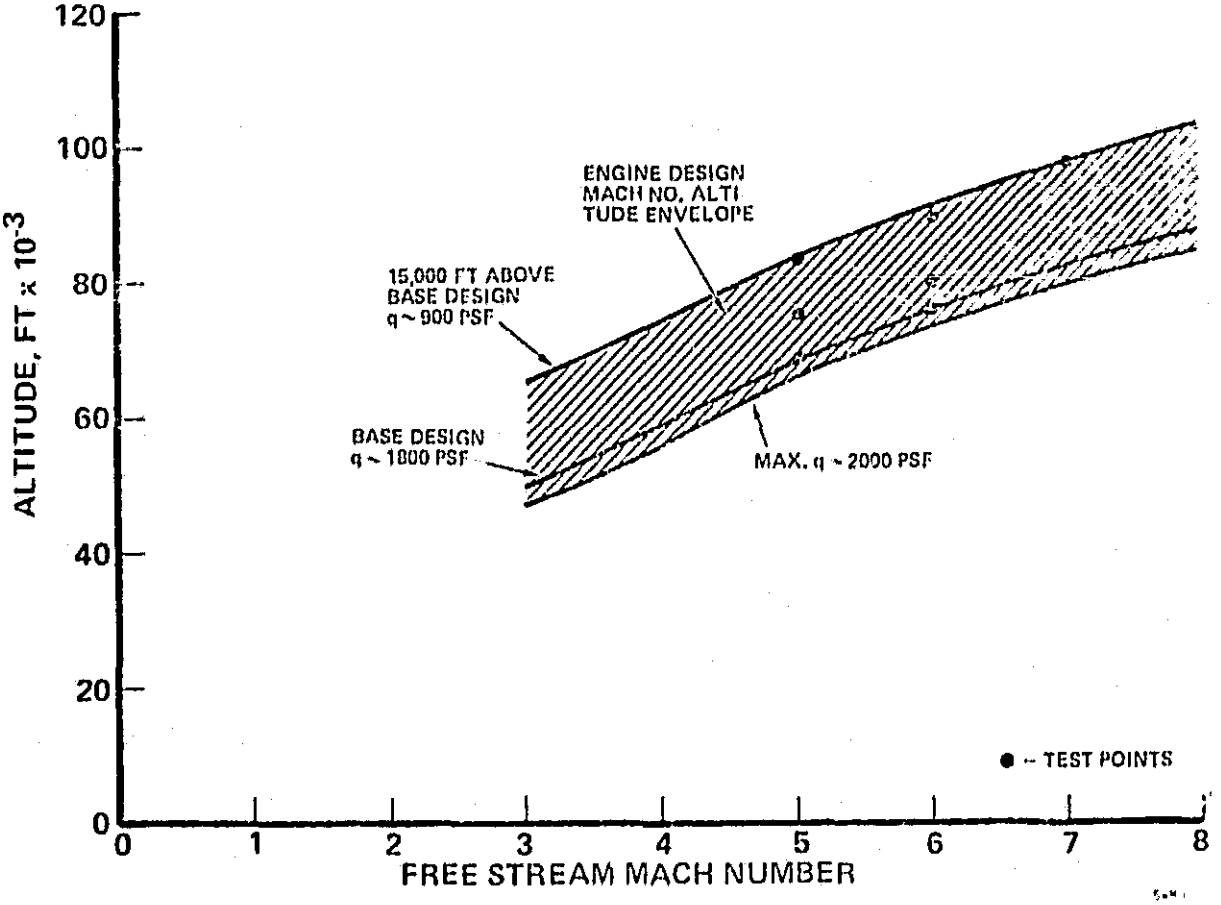

Fig. 7. Altitude Mach Number Envelope
Title (U), figure (U)

SUBSONIC AND SUPERSONIC COMBUSTION

(C) The AIM was designed to operate with subsonic combustion from Mach 3 to 6 and with supersonic combustion from Mach 6 to 8. At the transition Mach number of 6, no significant difference in engine thrust between the two combustion modes was expected. The test results shown in Figure 8 verified the original design concept. The top curves represent the pressure distribution on the outer-combustor surface and the bottom curves on the inner-combustor surface.

(C) Fuel was injected from the first and second stage injectors for the supersonic combustion test and from only the third stage injectors for the subsonic combustion test. It is interesting to note that even though the pressure distribution in the combustor varied between the two modes, the static pressures at the combustor exit were almost identical. With approximately the same combustor efficiency, the flow Mach number at the exit and thrust producing capability of the combustor were about the same. This was substantiated by the net thrust calculation indicated by the bar chart in the upper left corner of Figure 8.

COMPONENT PERFORMANCE

(U) Inlet. The inlet performance was compared with component test data and theoretical values in Figure 9. The static pressure rise showed excellent agreement on the inlet spike. The inlet cowl distribution showed that there was a steep pressure drop near the inlet throat. This favorable pressure gradient may have contributed to the lack of auto-ignition in the first stage during tests.

(C) The mass-momentum-energy method was used to determine inlet performance. The cumulative pressure integral and friction forces were added algebraically to the freestream momentum to obtain the momentum at the inlet throat. The following was the mass-momentum-energy averaged values obtained at Mach 6:

		Component	
	AIM Test	2/3 Scale Test	Theory (ref. 1)
Inlet Total Pressure Recovery	0.38 - 0.40	0.36-0.44	0.47
Reynolds Number	$1.4 - 2.8 \times 10^6$	$1.4 - 4 \times 10^6$	1.4×10^6

Reynolds number was based on inlet cowl diameter. AIM test data agreed fairly well with both the 2/3 scale model tests and theory.

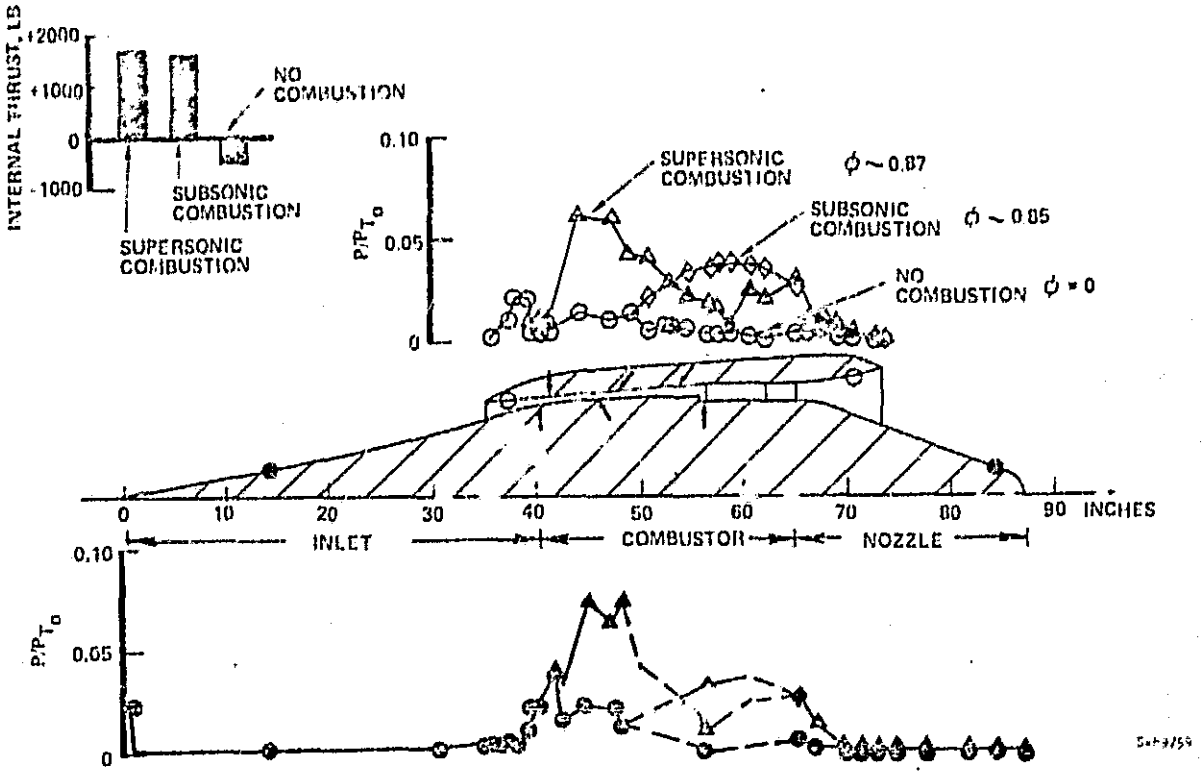

Fig. 8. Subsonic and Supersonic Combustion
Title (U), figure (C)

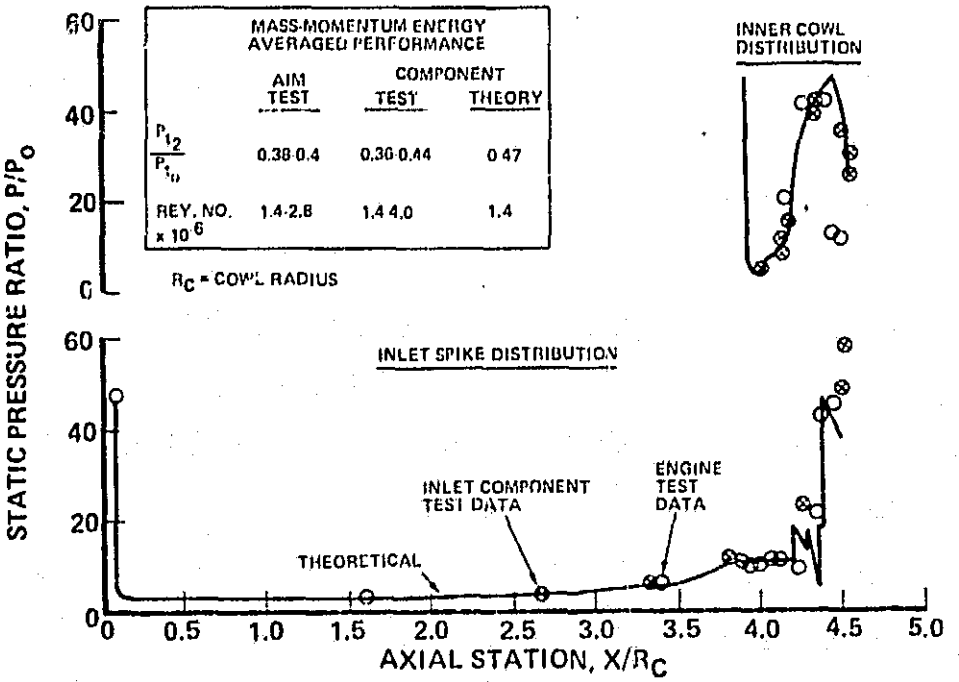

ORIGINAL PAGE IS
OF POOR QUALITY

Fig. 9. Inlet Pressure Distribution
Title (U), figure (C)

(C) Combustor. Detailed combustor performance for the AIM tests was presented in Reference 5. Combustor efficiencies up to 95 percent were obtained. The combustor efficiency is defined as the mass fraction of injected fuel reacted in equilibrium to satisfy the one-dimensional conservation equations. Combustor efficiency for all of the injectors tested versus equivalence ratio is shown in Figure 10. The efficiency was high and as anticipated, varied with the particular injectors used. The combustion process in the AIM (total pressure recovery of 14 percent) is better than that of a constant pressure process at an equivalence ratio of unity as shown in Figure 11.

(U) Nozzle. A convenient parameter used to define the performance of the nozzle is the vacuum stream thrust coefficient, C_s, defined as:

$$C_s = \frac{\text{Actual nozzle exit momentum}}{\text{Ideal nozzle exit momentum}}$$

Ideal nozzle exit momentum was calculated from an isentropic expansion of the combustor exit flow in chemical equilibrium.

(U) Two methods were used to obtain the actual nozzle exit momentum. The first method used the pressure integral on the nozzle surfaces and the calculated friction force. The second method used thrust measurements with actual exit momentum (F4) equal to:

$$F_4 = F_c + F_{ext} + F_{cav.} + F_o$$

where F_c = Corrected load cell force

F_{ext} = Total external pressure and friction forces

F_{cav} = Cavity force

F_o = Freestream momentum

(U) A correlation of the nozzle performance was obtained as shown in Figure 12. The two methods gave a range of stream thrust coefficients. Considering the errors involved in the calculations, the average of the upper and lower values appears as the most probable nozzle stream thrust coefficient.

(U) Table I gives a comparison of actual and predicted nozzle performance including a loss breakdown. The divergence and kinetics losses were based on theoretical calculations (Ref. 4, 6). The friction and heat losses were obtained from the test data.

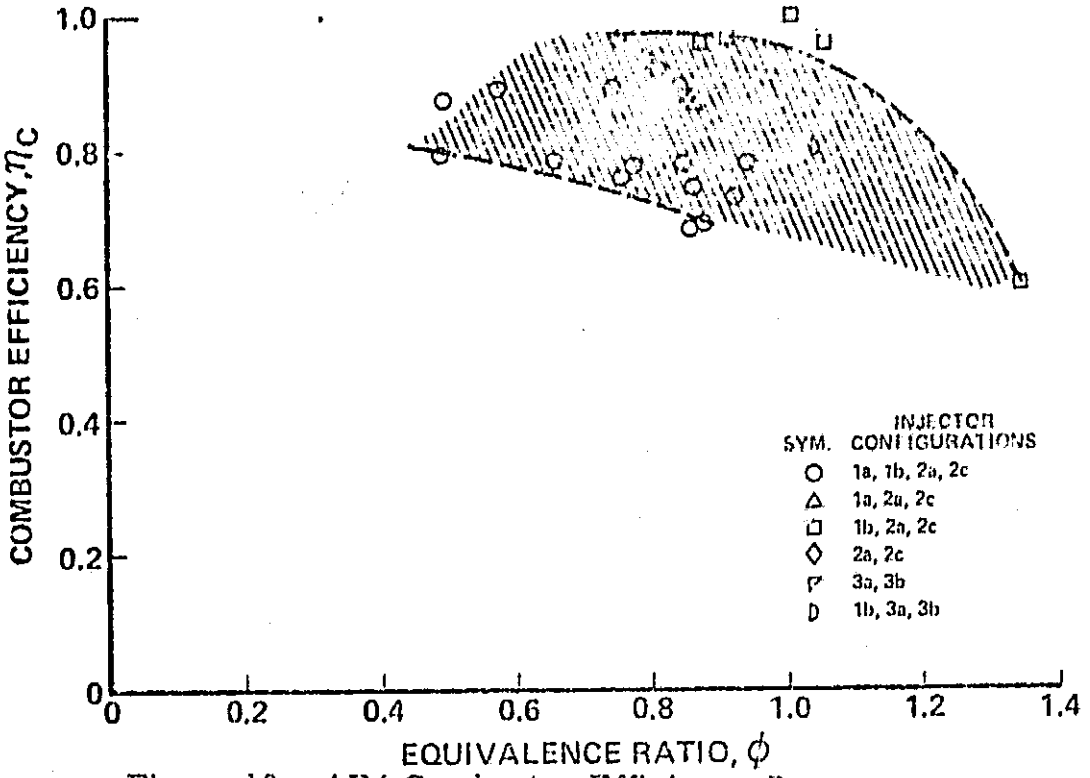

Figure 10. AIM Combustor Efficiency Range
Title (U), figure (C)

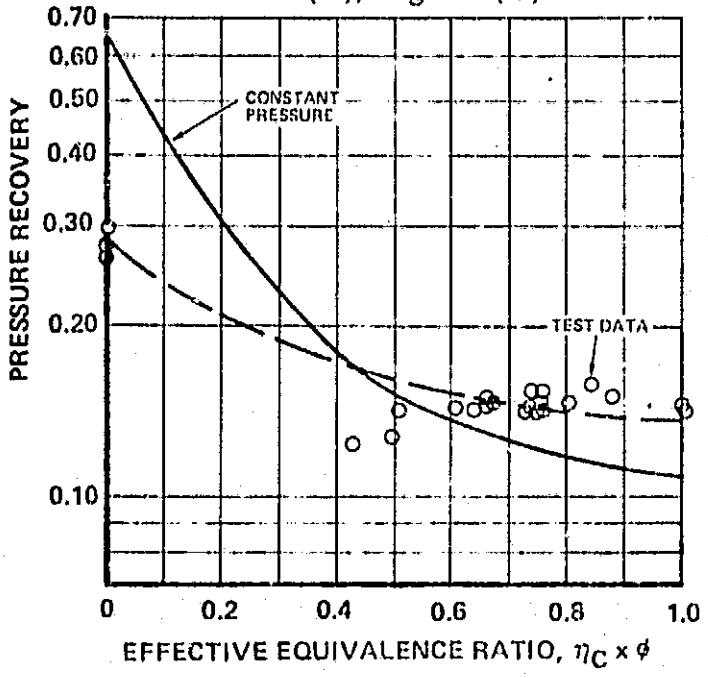

Figure 11. Combustor Total Pressure Recovery
Title (U), figure (C)

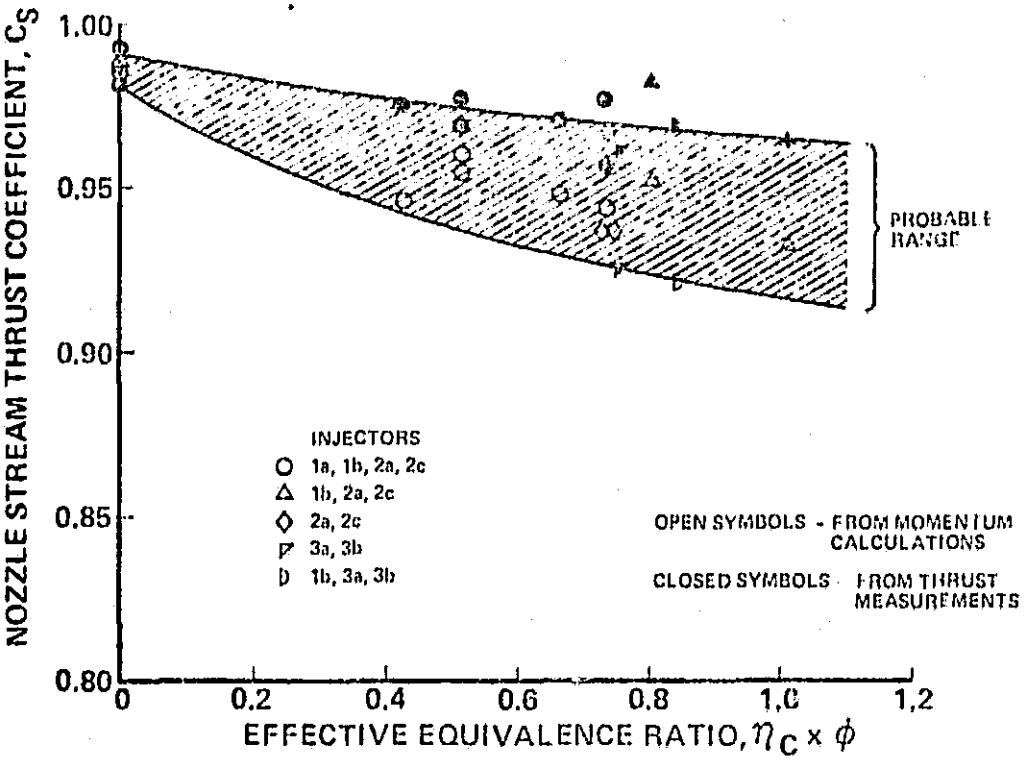

Figure 12. Nozzle Performance
Title (U), figure (C)

TABLE I

NOZZLE LOSSES (PERCENT) (C)

	Measured $\phi = 0$	Measured $\phi = 1$	Predicted $\phi = 1$
Cs Avg. (Fig. 12)	0.985	0.940	0.970
Loss Breakdown:			
Divergence and Friction	0.012	0.012	0.01
Configuration	0.005	0.005	0.005
Heat Loss	0.005	0.012	0.005
Kinetics Effects	---	0.010	0.010
Total Loss	0.022	0.039	0.030
Cs (from breakdown)	0.978	0.961	0.97

(C) There was a trend of decreasing performance with increasing equivalance ratio. At an equivalence ratio of zero, the measured C_s of 0.985 agrees closely with the calculated value of 0.978 from the nozzle loss breakdown. At an equivalance ratio of unity, both the predicted C_s and that calculated from a loss breakdown are higher than the measured value of 0.94. Of the difference in performance of about 4.5 percent between an equivalence ratio of zero and unity, approximately 2 percent can be accounted for by increased heat loss and kinetics effects. The remainder may be attributable to flow swirl. Swirl was evident in three different locations. The metal surface in the wake downstream of several struts showed a noticeable swirl (from the colored heat patterns) as much as 10 degrees. Swirl was also evident from the heat patterns on the leading edge of the struts and from the shock patterns on the surface of the instrumentation rig just upstream of the sampling probe tubes. A typical view of the unsymmetrical shock pattern is shown in Figure 13. Further investigation is needed in order to verify the qualitative findings of swirl which can seriously impair the overall engine performance.

(U) Engine Cycle and Efficiencies. The engine cycle may be illustrated by a temperature-entropy diagram as shown in Figure 14 for a typical supersonic combustion case. The air was decelerated in the inlet along path 0-2. The combustion process occurred along path 2-3. The saw-tooth-shaped curve indicates the fuel injection and heat release processes. Expansion of hot gas occurred through the nozzle (path 3-4) with a further increase in entropy.

(U) It is interesting to note that the entropy increase after each fuel injection is quite significant even before the total temperature rise. This indicates that large losses were associated with fuel-air mixing, flow shocks, mass addition and momentum change (upstream fuel injection). The flow velocities at different stations are also shown. The minimum velocity of 3900 ft/sec was noted at the combustor exit. The calculated total flow residence time is approximately 1/2 millisecond which makes the mixing and combustion a very difficult problem in a hypersonic ramjet system. The ratio of the kinetic energy produced to the theoretical energy addition is defined as the thermal efficiency, η_{th}.

$$\eta_{th} = \frac{\Delta K.E._{effective}}{w_f\left(H.V. + \frac{V_\infty^2}{2g} + H_f\right) - Q_{LOSS}}$$

where $$\Delta K.E._{effective} = \frac{W_{air}}{2g}\left[\left(1 + \frac{f}{a}\right)V_{ef}^2 - V_\infty^2\right]$$

H.V. = heating value of fuel,

H_f = fuel enthalpy $\qquad$ Q_{LOSS} = total engine heat loss

Figure 13. Unsymmetrical Shock Pattern at Combustor Exit
Title (U), figure (U)

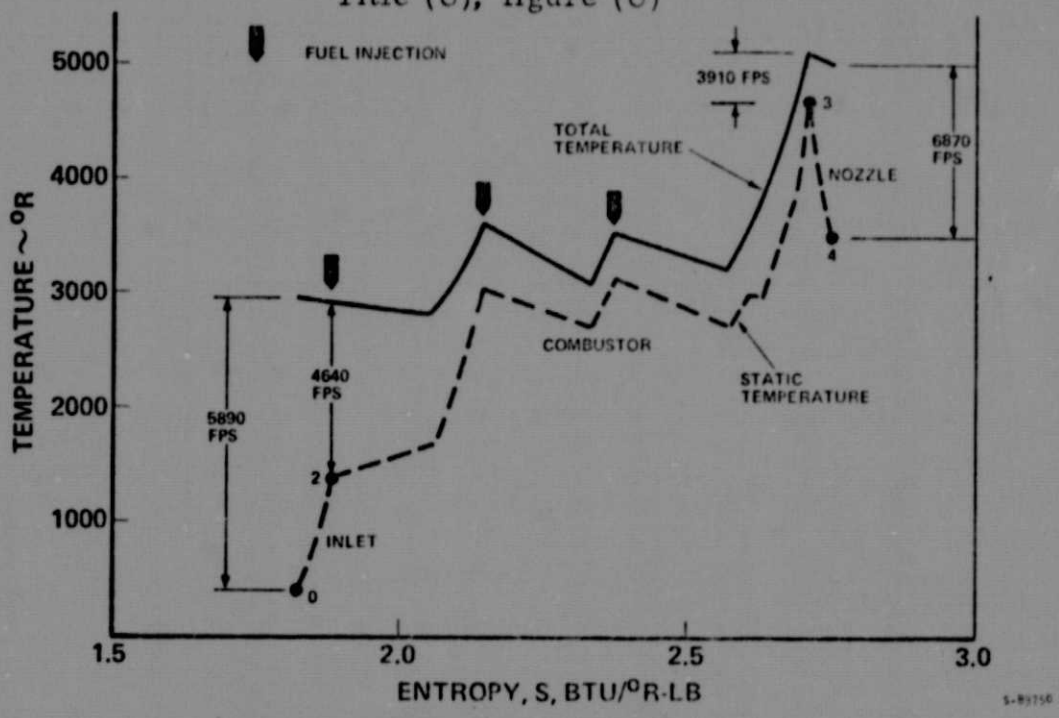

Figure 14. Temperature-Entropy Diagram for Supersonic Combustion
Title (U), figure (C)

and $$V_{ef} = V_e + \frac{gA_e P_e}{W_{air}\left(1 + \frac{f}{a}\right)}$$

The term $\frac{V_\infty^2}{2g}$ in the denominator of η_{th} accounts for the kinetic energy of fuel carried aboard the airplane.

(U) The ratio of the useful internal propulsive work to the increase in kinetic energy is defined as the propulsive efficiency, η_p

$$\eta_p = \frac{T_i V_\infty}{\Delta K.E._{effective}} \qquad T_i = \text{internal thrust}$$

The overall efficiency η_o is defined as the ratio of propulsive work to the theoretical ideal energy addition,

$$\eta_o = \eta_p \eta_{th} = \frac{T_i V_\infty}{W_f\left(H.V. + \frac{V_\infty^2}{2g} + H_f\right) - Q_{loss}}$$

The efficiencies at various fuel-air ratios are tabulated in Table II.

TABLE II

ENGINE EFFICIENCIES (C)

f/a	ϕ	η_p	η_{th}	η_o
0.0311	1.06	0.85	0.39	0.33
0.0250	0.850	0.86	0.36	0.31
0.0164	0.491	0.86	0.30	0.26

OVERALL ENGINE INTERNAL PERFORMANCE

(U) Determination of Internal Thrust. The internal thrust, Ti, is defined as the net sum (in a direction parallel with and opposed to the entering airstream) of the absolute pressure and friction imposed by the fluids passing through the engine on the physical parts of the engine (Ref. 7). The engine internal thrust was determined by two independent methods. The first method used the thrust measurements corrected with the external drag force and cavity force. Both of these forces were in

the same order of magnitude as the internal thrust force. The external drag force was large because of the steep outer cowl angle, and a high pressure zone which existed between the outer cowl and the tunnel shroud when fuel was injected. The cavity force was caused by the unbalanced forces from purge nitrogen flow in the AIM cavity between the engine shroud and the outerbody. The second method used a direct calculation ($\int PdA$) and the calculated friction force (Ref. 8) and fuel momentum. The equations used were:

$$(1) \quad T_i = F_c + F_{ext.} + F_{cav.}$$

and

$$(2) \quad T_i = \int PdA - F_{fuel} - F_{friction}$$

with

T_i = internal thrust

F_c = corrected load cell force

F_{ext} = total pressure and friction external force

F_{cav} = cavity force

$\int PdA$ = internal engine surface pressure integral

F_{fuel} = fuel momentum

$F_{friction}$ = internal friction force

(U) The commonly used thrust differential method which determines the thrust increment between hot and cold runs was not employed. This method assumes that the external forces are invariant during the run and would have caused serious errors if not carefully examined.

(C) Thrust from Measurements and Momentum Consideration. The comparison of internal thrust calculated from these two methods for a typical case is shown in Figure 15. The calculated total internal friction force was 440 pounds--about 25 percent of the internal thrust. Fuel injected at angles greater than 90 degrees to increase mixing efficiency caused a loss in engine thrust of about 100 pounds or 5 percent of the internal thrust.

(U) For the data shown in Figure 15, the internal thrust calaculated by the two methods agreed within 11 percent.

(U) The internal performance of the AIM engine in terms of thrust coefficient and specific impulse was defined as follows:

$$\text{Thrust Coefficient } (C_T) = \frac{\text{Internal thrust}}{q_o \ A_c}$$

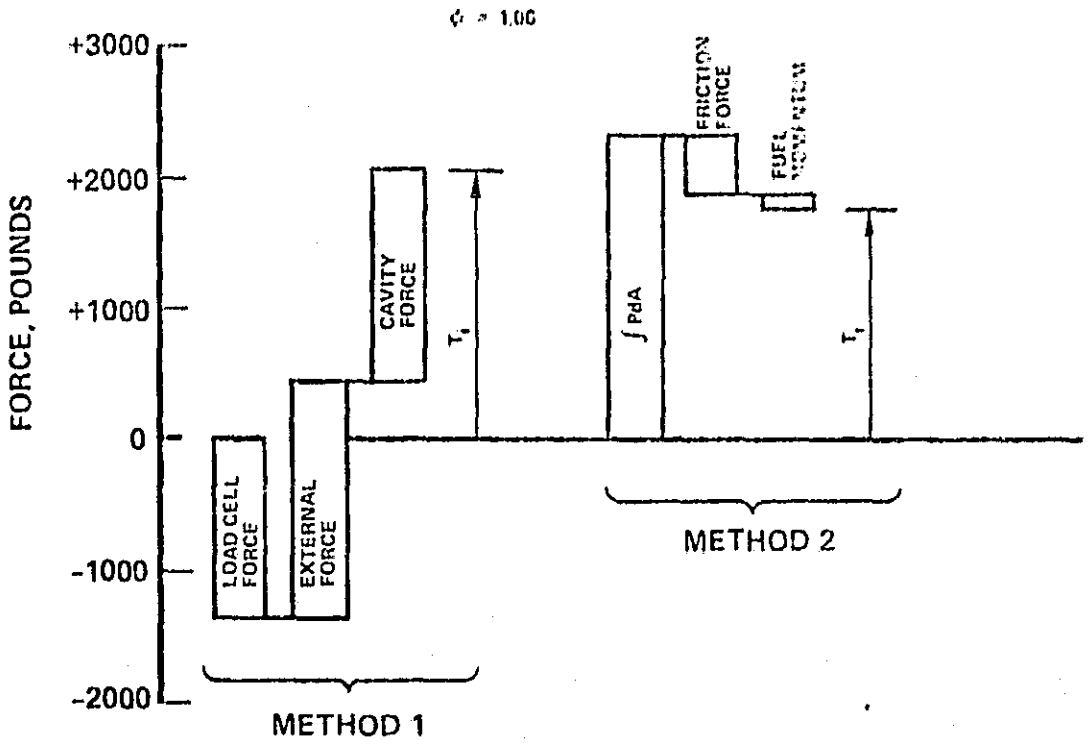

Figure 15. Comparison of Thrust Calculations
Title (U), figure (C)

$$\text{Fuel Specific Impulse } (I_{sp}) = \frac{\text{Internal thrust}}{\text{fuel flow}}$$

where q_o = freestream dynamic pressure, psia

and

A_c = engine cowl area, 256.13 in.^{2}

(U) The dynamic pressure was calculated from freestream properties and the fuel flow was measured during tests.

(U) The thrust coefficient and specific impulse were calculated from the two methods discussed above and plotted in Figure 16 over the range of fuel air ratios. Thrust coefficient was plotted versus fuel-air ratio rather than equivalence ratio because the composition of synthetic air was varied from run to run. For the majority of tests, data calculated from the thrust measurements agreed with that from surface pressure integrals within 10 percent.

(U) Thrust Distribution. In Figure 17, the contribution of forces from the AIM inlet, combustor and nozzle on engine thrust is illustrated at an equivalence ratio near unity. The diverging area combustor contributed about the same thrust as the nozzle. Engine internal thrust was determined from the

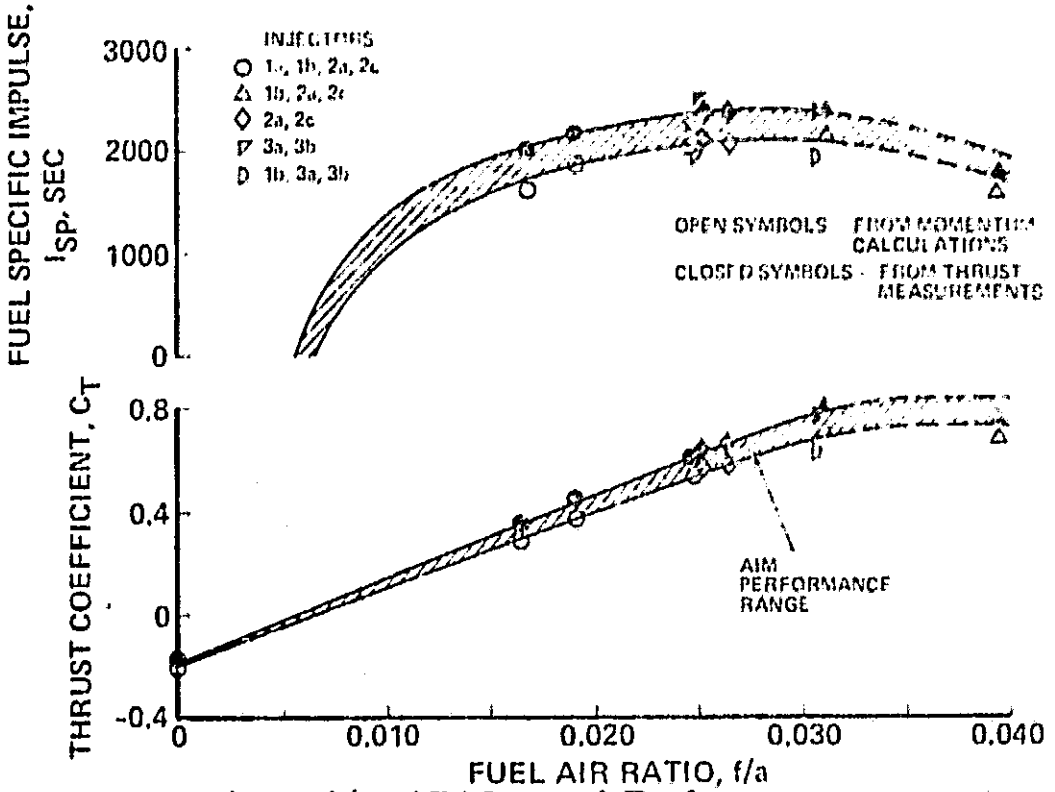

Figure 16. AIM Internal Performance
Title (U), figure (C)

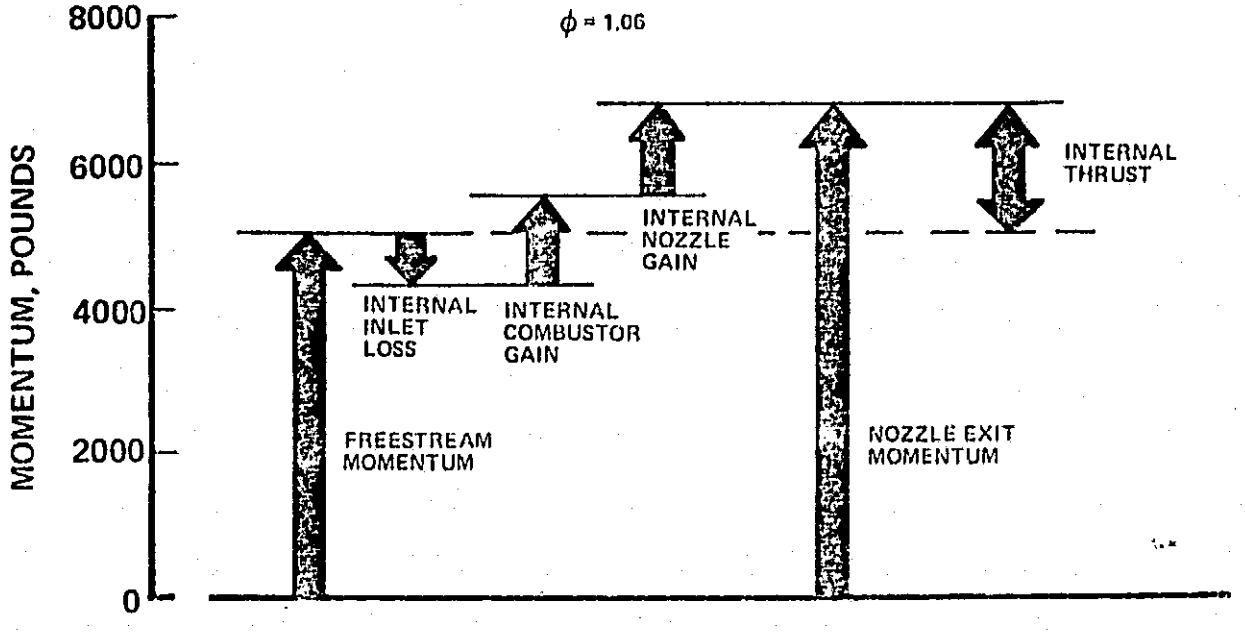

Figure 17. Thrust Distribution AIM Force Distribution
Title (U), figure (C)

difference between two large values--freestream and nozzle exit momentum. In this case, the gross thrust is approximately four times the engine internal thrust at Mach 6. Thus small errors in either of these values can provide large errors in engine internal thrust.

(U) Determining accurate component performance from engine tests is usually difficult. However, the close comparison of engine thrust from load cell readings with that calculated from momentum considerations (Figure 16) has increased the confidence of calculated component performance.

(U) Performance. The state-of-the-art for the hypersonic ramjet performance is shown in Figure 18. The cross-hatched regions represent the theoretically predicted performance for AIM. The closed circular symbol represents the AIM test results. The data was not corrected for the regeneratively cooled system because a very small correction was needed with fuel heated up to 1500°R.

(U) Other symbols shown in this figure were obtained from other sources (Ref. 9, 10, and 11). It should be noted that the basis for comparison between AIM performance and that from the other sources may not be the same. For a fair comparison differences such as fuel temperature, inlet air enthalpy, composition, and wall surface temperature must be considered. This chart, however, indicates the performance levels which have been demonstrated for hypersonic ramjets.

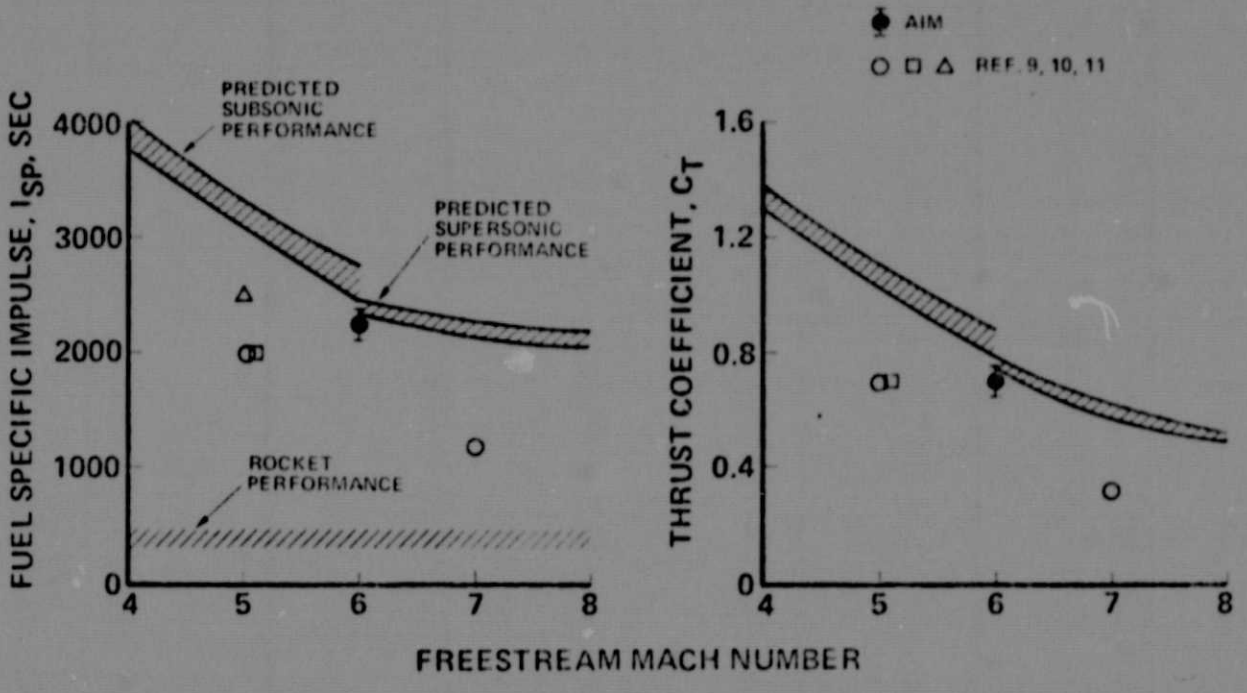

Figure 18. Hypersonic Ramjet Performance
Title (U), figure (C)

CONCLUSIONS (C)

1. Stable subsonic and supersonic combustion and convertibility were achieved over a range of equivalence ratios at Mach 6. No significant performance difference was observed between these two modes of operation.

2. Inlet total pressure recovery of 40 percent agreed very well with the theoretical prediction. Combustor efficiency of 95 percent was achieved in a length of 25.5 inches. Nozzle performance with C_s equal to 94 percent is lower than predicted.

3. Specific impulse of 2250 seconds and a corresponding thrust coefficient of 0.7 were demonstrated.

4. Internal engine thermal efficiency of 0.39, internal propulsive efficiency of 0.85 and overall efficiency of 0.33 were obtained at an equivalence ratio of unity.

5. Further investigation of combustor flow swirl problem is needed to verify the qualitative findings from this test. Significant performance improvement may be achieved by alleviating this problem.

REFERENCES

1. Engineering Staff, "Hypersonic Research Engine Project - Phase IIA Inlet Program, Final Technical Data Report (U) 1 March 1967 through 28 Feb. 1969, NASA Contract No. NAS1-6666, AiResearch Document No. AP-69-4883.

2. Engineering Staff, Hypersonic Research Engine Project - Phase II, Aerothermodynamic Integration Model Development Seventh Interim Technical Data Report, 10 September through 9 December 1969, NASA Contract No. NAS 1-6666, AiResearch Document No. AP-69-5899.

3. Engineering Staff, "Hypersonic Research Engine Project - Phase IIA Nozzle Program, Terminal Summary Report (U) 14 June 1967 through 3 September 1968, NASA Contract No. NAS1-6666, AiResearch Document No. AP-68-4451, 17 Dec. 1968.

4. Gaede, A. E., and Lopez, H. J., "Selection of Nozzle Contours for a Research Scramjet Engine," AIAA Paper No. 67-453 presented at AIAA 3rd Propulsion Joint Specialist Conference, July 17-21, 1967.

5. Sun, Yung H., Gaede, Albert E., and Sainio, Walter C., "Some Combustor Test Results of NASA Aerothermodynamic Integration Model (AIM/HRE), paper presented at 11th Jannaf Combustion Meeting, 9-13 September 1974, also NASA CR 132525

6. Engineering Staff, "Hypersonic Research Engine Project - Phase II, Aerothermodynamic Integration Model Measurement Plan," NASA Contract No. NAS1-6666, AiResearch Document No. AP-70-0210, 9 June 1970.

7. Langley Research Center, "Conceptual and Preliminary Design of the Hypersonic Ramjet," Statement of Work, Exhibit A, L-4047, April 15, 1965.

8. Spalding, D.B., and Chi, S.W., "Drag of a Compressible Turbulent Boundary Layer on a Smooth Flat Plate With and Without Heat Transfer," Journal Fluid Mechanics, Vol. 18, Pt. 1, Jan 1964, pp 117-143.

9. Bahr, D.W., Kenworthy, M.J., Hollmer, W., and King, R.C., "Scramjet Exploratory Development Program (U)", General Electric, Cincinnati, Ohio, September, 1969, NASA Contract NAS1-6544.

10. McFarlin, D.J., Kepler, C.E. "Mach 5 Test Results of Hydrogen-Fueled Variable-Geometry Scramjet", Technical Report AFAPL-TR-68-116 October, 1968, United Aircraft Research Laboratories.

11. Burnette, T.D., "Dual Mode Scramjet Part III Engine Design and Performance Characteristics", AF APL-TR-67-132, Part III, June, 1968

6. Engineering Staff, "Hypersonic Research Engine Project - Phase II, Aerothermodynamic Integration Model Measurement Plan, NASA Contract No. NAS1-6666, AiResearch Document No. AP-70-6216, 9 June 1970.

7. Langley Research Center, "Conceptual and Preliminary Design of the Hypersonic Ramjet," Statement of Work, Exhibit A, L-4947, April 15, 1965.

8. Spalding, D. B., and Chi, S. W., "Drag of a Compressible Turbulent Boundary Layer on a Smooth Flat Plate With and Without Heat Transfer," Journal Fluid Mechanics, Vol. 18, Pt. 1, Jan 1964, pp 117-143.

9. Bahr, D. W., Kenworthy, M. J., Hollmer, W., and King, R. C., "Scramjet Exploratory Development Program (U)", General Electric, Cincinnati, Ohio, September, 1969, NASA Contract NAS1-8544.

10. McFarlin, D. J., Kepler, C. E. "Mach 5 Test Results of Hydrogen-Fueled Variable-Geometry Scramjet", Technical Report AFAPL-TR-68-116 October, 1968, United Aircraft Research Laboratories.

11. Burnette, T. D., "Dual Mode Scramjet Part III Engine Design and Performance Characteristics", AF APL-TR-67-132, Part III, June, 1968